Electronic Supplementary Material (ESI) for Journal of Materials Chemistry A.


# SUPPLEMENTARY INFORMATION

# Tailoring the efficiency of porphyrin molecular frameworks for the electroactivation of molecular $N_2$

María Romero-Angel,[a] Roumayssa Amrine,[b] Beatriz Ávila-Bolívar,[b] Neyvis Almora-Barrios,[a] Carolina R. Ganivet,[a] Natalia M. Padial,[a] Vicente Montiel,[b] José Solla Gullón,[*b] Sergio Tatay[*a] and Carlos Martí-Gastaldo[*a]

[a] Instituto de Ciencia Molecular (ICMol). Universitat de València, Catedrático José Beltrán-2, 46980, Paterna, Spain.

[b] Instituto de Electroquímica, Universidad de Alicante, Apdo. 99, E-03080, Alicante, Spain.

# S1. MATERIALS AND REAGENTS

Dichloromethane (>99%), Boron trifluoride diethyl etherate ($BF_3{\cdot}OEt_2$, >46.5%), Cobalt(II) chloride hexahydrate ($CoCl_2{\cdot}6H_2O$, 98%), Copper(II) chloride dihydrate ($CuCl_2{\cdot}2H_2O$, >99%), Nickel(II) chloride hexahydrate ($NiCl_2{\cdot}6H_2O$, 99.9%), Ethyl acetate (>99.5%), *N,N*-Dimethylformamide (99.8%), Chloroform-D (99.8%), Potassium bicarbonate ($KHCO_3$, 99%), Sodium sulfate ($Na_2SO_4$, 93%) and 4-formyl benzonitrile (95%) were purchased from Sigma-Aldrich, *p*-chloranil (99%), Tetrahydrofuran (>99%) and Boron tribromide solution 1 M in methylene chloride ($BBr_3$) were purchased from Acros Organics, pyrrole (>98%), *N,N*- Diethylformamide (99%), Methanol (99%) and Hexane were purchased from Alfa Aesar, Methyl 4-formyl-3-fluorobenzoate and 5,10,15,20-Tetrakis(4-carboxyphenyl)porphyrin were purchased from BLD pharma, Acetic acid ($CH_3COOH$), Silica gel and Potassium hydroxide (KOH, 85%) were purchased from Thermo Fisher Scientific. All reagents and solvents were used as received without further purification. $Na_2SO_4$ (99.5%, Fisher Chemical) was used as supporting electrolyte in the catholyte and anolyte solutions, while Sulfuric acid (95-97% Emsure ISO) was used for the $NH_3$ acid trap solution. A cationic ion exchange membrane Nafion 112, purchased from DuPont (Wilmington, DE, USA), and activated in 0.5 M NaOH (98.5% VWR chemicals), was used as a separator in the electrochemical H-cell. All other chemicals were purchased from the highest analytical grade available and were used as received without any further purification. All solutions were prepared using MilliQ ultrapure water (18.2 MΩ cm).

# S2. SYNTHESIS OF MATERIALS AND EXPERIMENTAL DETAILS

## S2.1. PHYSICAL AND CHEMICAL CHARACTERIZATION

**X-Ray Diffraction Patterns (PXRD) -** were collected in a PANalytical X'Pert PRO diffractometer using copper radiation (Cu Kα = 1.5418 Å) with an X'Celerator detector, operating at 40 mA and 45 kV. Profiles were collected in the 2° < 2θ < 40° range with a step size of 0.017°. XRD pattern for refinement was collected for polycrystalline sample using a 0.5 mm glass capillary mounted and aligned in a PANalytical Empyrean diffractometer (Bragg-Brentano geometry) using copper radiation (Cu Kα l= 1.5418 Å) with an PIXcel detector, operating at 40 mA and 45 kV. Profiles were collected by using a Soller Slit of 0.02° and a divergence slit of ¼ at room temperature in the angular range 3° < 2θ < 40° with a step size of 0.017°.

**Scanning Electron Microscopy (SEM) -** Particle morphologies and dimensions were studied with a Hitachi S-4800 scanning electron microscope at an accelerating voltage of 20 kV, over metalized samples with a mixture of gold and palladium for 90 seconds.

**$^1$H-Nuclear Magnetic Resonance (NMR) -** spectra were recorded on a Bruker Avance III 300 WB spectrometer and were calibrated to the residual solvent peak (DMSO at 2.500 ppm $^1$H-NMR) or (DMSO-$d_6$ at 2.50 ppm $^1$H-NMR). The following abbreviations were used to explain multiplicities: s = singlet, d = doublet, t = triplet, q = quartet, m = multiplet, br = broad. The analysis was carried out with the MestRenova software package.

**Gas sorption -** Surface area, pore size and volume values were calculated from nitrogen adsorption-desorption isotherms (77 K) recorded on a Micromeritics 3Flex apparatus. Samples were degassed overnight at 60 °C and $10^{-6}$ Torr prior to analysis. Brunauer-Emmett-Teller (BET) Surface area analysis were performed as recommended for microporous and mesoporous materials. Specific surface area was calculated by multi-point BET method. Pore size distributions (PSD) were estimated by NLDFT methods

assuming an oxide surface model with cylindrical shaped pores, which provided a good fit to the experimental data. Water adsorption isotherm at 298K was recorded on a Belsorp Max II apparatus.

**Fourier-transform Infrared spectroscopy** - FT-IR spectra of the solids were collected in the range 4000-350 $cm^{-1}$ with an Agilent Cary 630 FTIR Spectrometer equipped with an ATR module.

**UV–Visible Absorption Spectroscopy -** experiments were performed on a Jasco V-750 spectrophotometer. UV-Vis measurements of the linkers were carried out by dissolving sample powders in the smallest amount of DMSO possible and then completing to a total volume of 3 mL of acetone to achieve a concentration of 0.3 mg mL-1. All the measured spectra exhibit intense Soret bands at ~410 nm and weaker Q bands in the range of ~500 nm-600 nm.

**Mass Spectroscopy with MALDI ionization source and time-of-flight analyzer (MS MALDI TOF) -** Samples were analyzed in a 5800 MALDI TOF/TOF (ABSciex) in reflector positive and negative mode, in a range 300 – 1500 m/z, at 2800 – 3500 of laser intensity.

**Elemental analysis (EA) –** Carbon, nitrogen and hydrogen contents were determined by microanalytical procedures using a LECO CHNS.

**Inductively coupled plasma Spectroscopy (ICP) -** the measurements were carried out with an Agilent 7900 apparatus.

**Electrode preparation -** In order to apply the catalyst to the electrode surface, a catalytic ink was prepared containing the samples previously synthesized, Nafion solution (perfluorosulfonic acid - PTFE copolymer 5% w/w solution, Alfa Aesar) as binder with a Catalyst:Nafion mass ratio of 80:20, and diluted to 2 wt% in absolute ethanol (EMSURE®, Merck, Darmstadt, Germany). The mixture was sonicated for at least 30 min and the ink was directly sprayed by air brushing technique onto a Toray paper (TGPH-90) from QuinTech, Göppingen, Germany) with a geometric surface area of 6.25 $cm^2$ (2.5 cm x 2.5 cm). The airbrush spraying is carried out on a hot metal plate at 90 °C to accelerate solvent evaporation. The final loading of the sample is about 0.7 $mg/cm^2$.

**Electrochemical characterization -** The electrochemical characterization of the prepared electrodes was performed in a three-electrode configuration glass cell in Ar and $N_2$-saturated 0.1 M $Na_2SO_4$ (99.5%, Fisher Chemical) solution using a platinum wire and a leakless AgCl/Ag (Saturated KCl) as counter and reference electrodes, respectively. Cyclic voltammetry (CV) experiments were performed using a PGSTAT302N system (Metrohm Autolab B. V., Utrecht, Netherlands). All CV measurements were performed at room conditions. Portions of about 3 $cm^2$ of the different electrodes were used during the electrochemical measurements. The current density was normalized by the geometric area of the electrodes. The electrode potentials were referred to the reversible hydrogen electrode (RHE) scale according to the equation:

$$E_{RHE} = E_{AgCl/Ag} + 0.059\, pH + E^{o}_{AgCl/Ag}$$

Where $E°_{AgCl/Ag}$= 0.197 V at 25 °C, pH= 6.15 (corresponding to 0.1 M $Na_2SO_4$ solution), and $E_{AgCl/Ag}$ is the applied potential against AgCl/Ag reference.

**Electrochemical synthesis of ammonia -** $N_2$ electroreduction was performed in an H-type electrochemical cell with divided compartments through a cationic ion exchange membrane (Nafion 112). A $N_2$-saturated 0.1 M $Na_2SO_4$ was used as catholyte and anolyte. A 1 mM $H_2SO_4$ solution was used to collect the $NH_3$ that

is present in the cathodic gas phase thus preventing the loss of any produced $NH_3$. The Nafion 112 membrane was previously activated in 0.5 M NaOH for 24 h. A platinum wire immersed in the anolyte acted as counter electrode. A leakless AgCl/Ag (Saturated KCl) electrode placed in the catholyte was used as reference electrode. The $N_2$ electroreduction electrolysis were carried out by setting at controlled potential between −0.04 V and −0.34 V vs RHE for 2 h using a PGSTAT302N system (Metrohm Autolab B. V., Utrecht, Netherlands). Moreover, two bubblers containing 0.1 M $KMnO_4$ and 0.1 M KOH were connected in series at the entrance of the cell to capture and prevent any NOx contaminations and false positives of $NH_3$ coming from the nitrogen gas cylinder[1-5]. It is also worth noting that all glassware was initially cleaned with a saturated $KMnO_4$ solution, to strip organic species, metals, and other $N_2$ species from the glassware. Then, the glassware is rinsed with a diluted $H_2O_2/H_2SO_4$ solution and finally boiled two-three times in ultrapure water.

## S2.2. SYNTHESIS

### S2.2.1. LIGAND SYNTHESIS

**5,10,15,20-Tetrakis(4-carboxyphenyl)-porphyrin** (**TCPP)** is commercially available.

**5,10,15,20-Tetrakis(4-carboxymethyl-fluorophenyl)-porphyrin methyl ester (TCPP-F methyl ester):**[6] In a foil-covered 2 L 2-neck flask equipped with a reflux condenser, magnetic stirrer, and a $N_2$ inlet was added Methyl 4-formyl-3-fluorobenzoate (1 g, 98%, 5.49 mmol), pyrrole (0.6 mL, 98%, 8.46 mmol), and $CH_2Cl_2$ (850 mL). The reaction mixture was stirred for 15 min at room temperature, then $BF_3{\cdot}OEt_2$ (105 µL, 0.85 nmol) was added. After 2 h, *p*-chloranil (1.56 g, 6.37 mmol) was added and the reaction mixture was heated at reflux for 2 h. The reaction mixture was evaporated to a volume of 50–100 mL, then absorbed onto silica gel (2.8 g). A purple solid was obtained in 25% yield. $^1$H NMR (300 MHz, $CDCl_3$) δ 8.23 (m, 12H), 4.12 (s, 12H), -2.85 (br s, 2H). Anal. Calc. for $C_{52}H_{36}F_4N_4O_4$: C 72.38, H 4.91, F 8.81, N 6.49; found: C 73.04, H 5.21, F 9.02, N 6.95. HRMS (ESI) *m*/*z*: $[M + H]^+$ calc. for $C_{52}H_{36}F_4N_4O_4$: 862.3142; found: 863.1760.

### Synthesis of *meta*-substituted MTCPPs methyl ester:

Metalation of the porphyrin core was carried out in a 50 mL round flask. There 0.33 mmol of TMPP and 1.82 mmol of each $MCl_2$ salt were dissolved in 15 ml of DMF and refluxed overnight. Then the mixture was washed with water and dried in vacuum at 60 C.

**(CoTCPP methyl ester)**: Anal. Calc. for $C_{52}H_{36}CoN_4O_4$: C 69.10, H 4.01, Co 6.52, N 6.20; found: C 71.09, H 4.76, Co 7.58, N 7.02. HRMS (ESI) *m*/*z*: $[M + H]^+$ calc. for $C_{52}H_{36}CoN_4O_4$: 899.1865; found: 900.6518.

**(CuMTCPP methyl ester)**: Anal. Calc. for $C_{52}H_{36}CuN_4O_4$: C 68.75, H 3.99, Cu 7.00, N 6.17; found: C 70.54, H 4.45, Cu 7.93, N 6.98. HRMS (ESI) *m*/*z*: $[M + H]^+$ calc. for $C_{52}H_{36}CuN_4O_4$: 903.1829; found: 904.4238.

**(NiTCPP methyl ester)**: Anal. Calc. for $C_{52}H_{36}N_4NiO_4$: C 69.12, H 4.02, N 6.20, Ni 6.50; found: C 71.24, H 4.86, N 6.79, Ni 7.22. HRMS (ESI) *m*/*z*: $[M + H]^+$ calc. for $C_{52}H_{36}NiN_4O_4$: 898.1887; found: 899.3294.

**(NiTCPP-F methyl ester)**: Anal. Calc. for $C_{52}H_{36}F_4N_4NiO_4$: C 69.11, H 3.98, N 6.18, F 8.83, Ni 6.55; found: C 70.44, H 4.26, N 6.82, F 9.01, Ni 6.82. HRMS (ESI) *m*/*z*: $[M + H]^+$ calc. for $C_{52}H_{36}F_4NiN_4O_4$: 974.1823; found: 975.1027.

## General procedure for the hydrolysis of TCPPs and MTCPPs methyl esters:

Methyl ester was hydrolyzed before each MOF synthesis by saponification. In a typical saponification 750 mg of TCPP were dissolved in 25 ml of THF and 25 ml of MeOH in a 100 ml round flask. Then KOH (2.63 g, 46 mmol) was added to 25 ml of deionized water and added to the above mixture. The mixture is refluxed overnight. Evaporate the THF and MeOH. Add water and then heat to dissolve the solid. Acidify with acetic acid while stirring until pH is neutral. Wash with water and dry in vacuum.

**5,10,15,20-Tetrakis(4-carboxymethyl-fluorophenyl)-porphyrin ($H_2$TCPP(F)):** A purple solid was obtained in 89% yield. $^1$H NMR (300 MHz, DMSO-$d_6$) δ 8.23 (m, 12H), 4.12 (s, 12H), -2.85 (br s, 2H). Anal. Calc. for $C_{48}H_{28}F_4N_4O_8$: C 67.97, H 3.73, F 8.27, N 6.10; found: C 69.34, H 4.01, F 8.82, N 6.89. HRMS (ESI) *m/z*: $[M + H]^+$ calc. for $C_{48}H_{28}F_4N_4O_8$: 918.2313; found: 919.9823.

**CoTCPP:** Anal. Calc. for $C_{48}H_{28}CoN_4O_8$: C 68.01, H 3.33, Co 6.95, N 6.61; found: C 69.87, H 3.72, Co 7.09, N 6.90. HRMS (ESI) *m/z*: $[M + H]^+$ calc. for $C_{48}H_{28}CoN_4O_8$: 847.1239; found: 848.1763.

**CuTCPP:** Anal. Calc. for $C_{48}H_{28}CuN_4O_8$: C 67.64, H 3.31, Cu 7.46, N 6.57; found: C 69.47, H 3.76, Cu 8.03, N 6.90. HRMS (ESI) *m/z*: $[M + H]^+$ calc. for $C_{48}H_{28}CuN_4O_8$: 851.1203; found: 852.4393.

**NiTCPP:** Anal. Calc. for $C_{48}H_{28}NiN_4O_8$: C 68.03, H 3.33, N 6.61, Ni 6.93; found: C 70.17, H 3.96, N 6.43, Ni 7.12. HRMS (ESI) *m/z*: $[M + H]^+$ calc. for $C_{48}H_{28}NiN_4O_8$: 846.1261; found: 847.7633.

**NiTCPP(F):** Anal. Calc. for $C_{48}H_{28}F_4NiN_4O_8$: C 68.05, H 3.32, F 8.91, N 6.68, Ni 6.91; found: C 69.27, H 3.78, F 9.02, N 6.43, Ni 7.03. HRMS (ESI) *m/z*: $[M + H]^+$ calc. for $C_{48}H_{28}F_4NiN_4O_8$: 922.1197; found: 923.1203.

NMR spectra of CoTCPP and CuTCPP are not included here because they are strongly perturbed by the magnetism of the $Co^{2+}$ and $Cu^{2+}$ core.

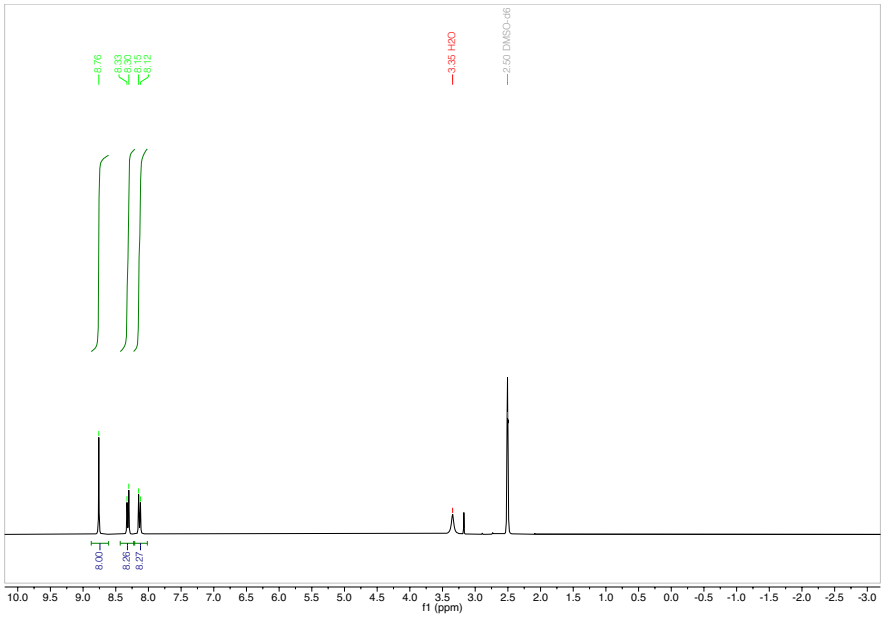


**Figure S1.** $^1$H-NMR (300MHz, DMSO) of $H_2$TCPP.

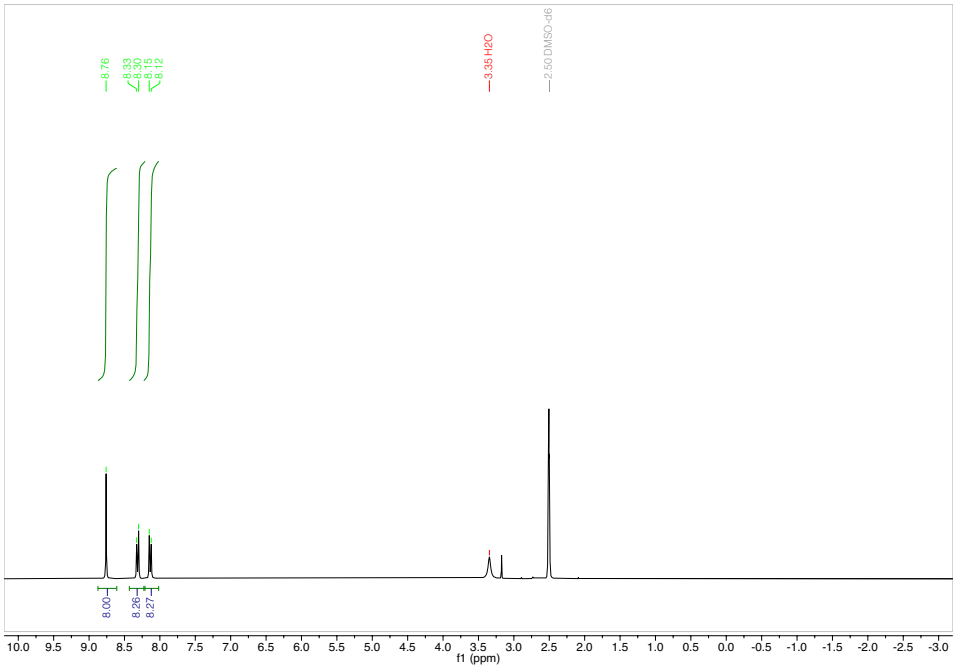


**Figure S2.** $^{1}$H-NMR (300MHz, DMSO) of NiTCPP.

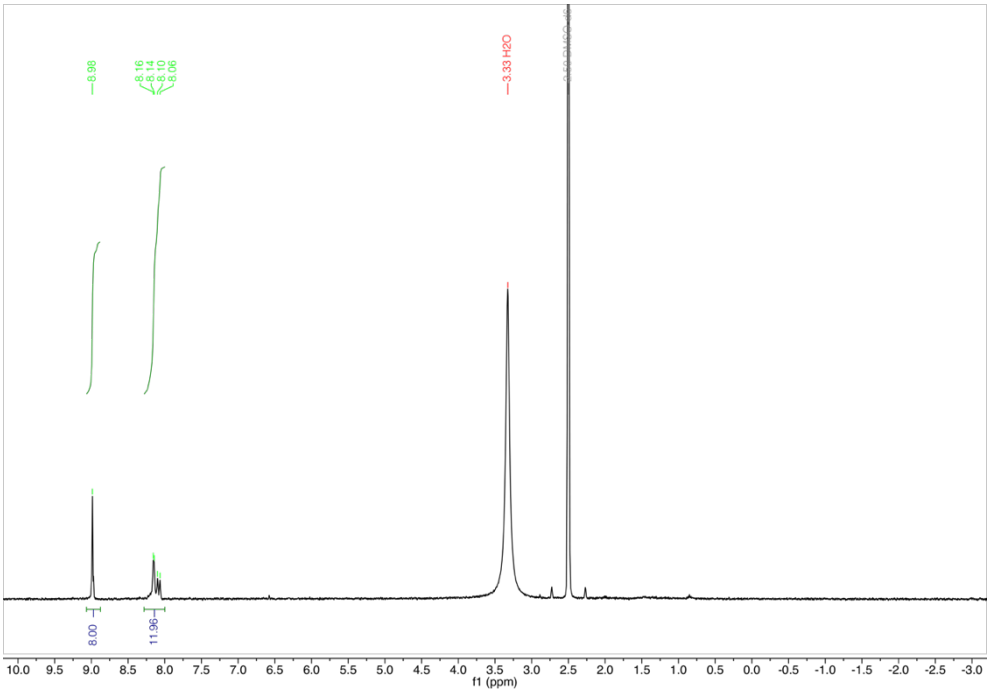


**Figure S3.** $^{1}$H-NMR (300MHz, DMSO) of NiTCPP(F).

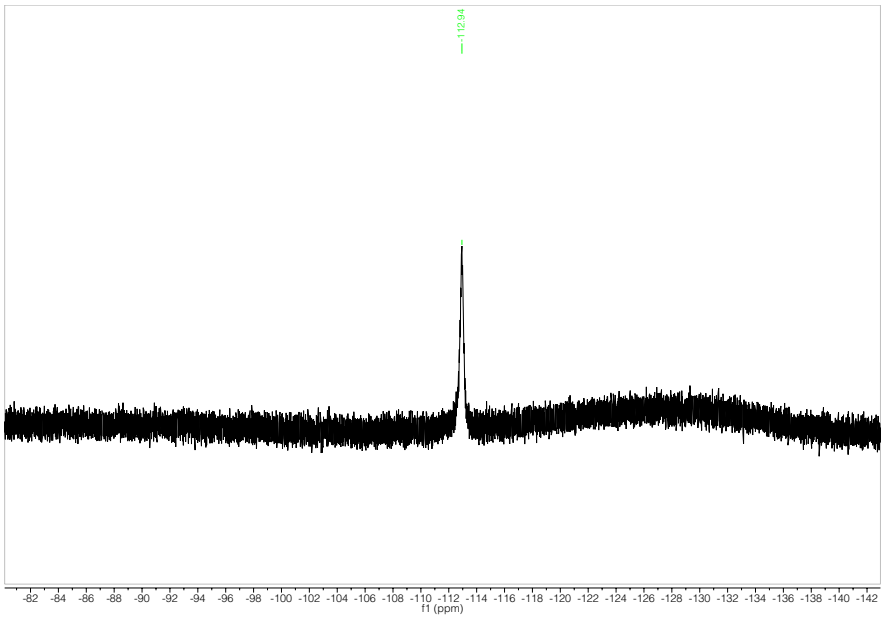


**Figure S4.** $^{19}$F-NMR (282MHz, DMSO) of NiTCPP(F).

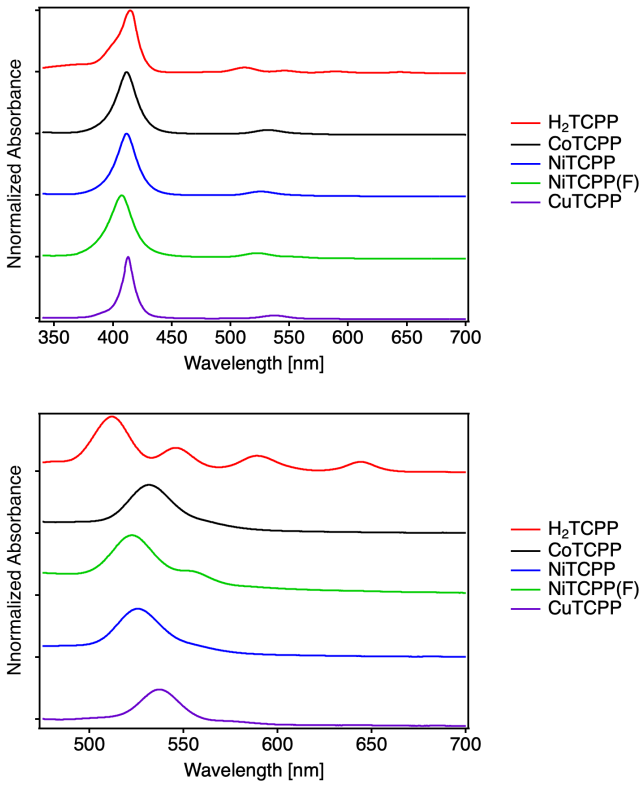


**Figure S5.** UV-Vis of $H_2$TCPP, MTCPP and NiTCPP(F) in acetone. The bottom figure shows a zoomed-in view of the region between 500 and 700 nm.

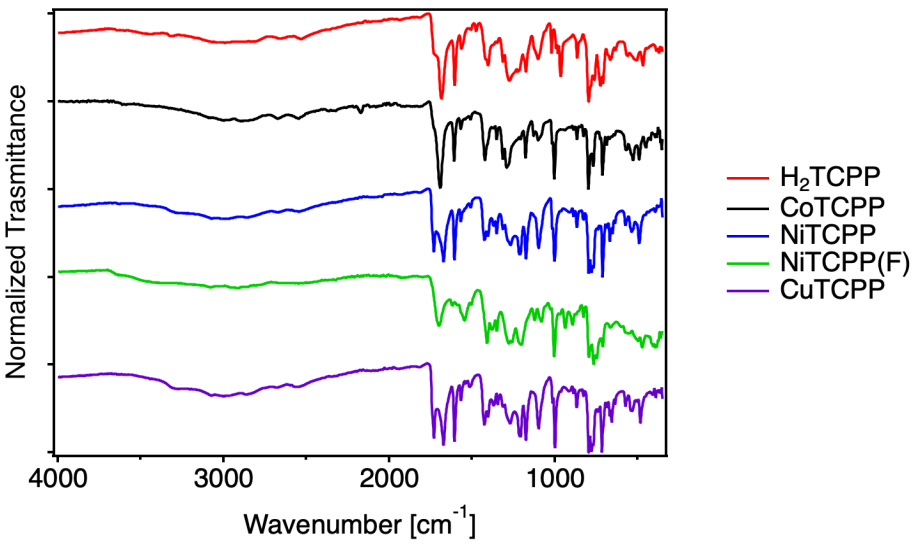


**Figure S6.** FT-IR spectra of $H_2$TCPP, MTCPP and NiTCPP(F).

## S2.2.2. MOF SYNTHESIS

**PCN-224:**[7] $ZrOCl_2 \cdot 8H_2O$ (188 mg, 0.582 mmol) and $H_2$TCPP (37.5 mg, 0.047 mmol) were dissolved in DMF (150 mL) via sonication. Acetic acid (37 mL, 647 mmol) was added, and the mixture was sonicated again. The reaction mixture was heated in an oven (72 h, 65 °C), washed with DMF (twice, 19k rpm/15 min/16 °C) and resuspended in 10 mL DMF. The suspension was activated with 8M HCl (8M, 0.5 mL) in an oven (15h, 100°C). The product was collected by centrifugation and washed with DMF (twice, 16k rpm/20 min/14 °C) and acetone (twice, 16 krpm/8 min/14 °C). The mixture was soaked in acetone 8 overnight and washed with acetone one more time. Centrifugation (16k rpm/5 min/14 °C) and drying for 3 h at room temperature yielded a purple powder as product.

**PCN-226:**[8] 0.9 mmol $ZrCl_4$ (0.21 g, 0.09 mmol), $H_2$TCPP (70 mg, 0.087 mmol) and benzoic acid (7.0 g, 57 mmol) in 14 mL of DMF were ultrasonically dissolved in a 20 mL Pyrex vial. The mixture was heated in 140 ºC oven for 72 h. After cooling down to room temperature, needle shaped crystals were harvested by centrifugation followed by washing by acetone.

**MOF-525:**[9] $ZrOCl_2 \cdot 8H_2O$ (12.5 mg, 0.037 mmol) was added to DMF (10 mL) and sonicated for thirty minutes. Following sonication, $H_2$TCPP (2.5 mg, 0.037 mmol) was added to the solution. After ten minutes further sonication, acetic acid (2.5 mL) was added to the solution. The solution was placed in a 20 mL scintillation vial and heated at 65 °C for three days. The microcrystalline powder was filtered and washed with DMF (5 × 10 mL) over a three-hour period. The DMF was then replaced with acetone (5 × 30 mL) over a five-day period. Finally, the volatile acetone was removed by heating at 120 °C under vacuum (30 mTorr) for 48 hrs.

**PCN-222:**[10] $ZrCl_4$ (75 mg, 0.032 mmol), H2TCPP (50 mg, 0.062 mmol) and benzoic acid (2700 mg, 0.022 mmol) in 8 mL of DEF were ultrasonically dissolved in a 20 mL Pyrex vial. The mixture was heated in 120 ºC oven for 48 h. After cooling down to room temperature, purple needle shaped crystals were harvested by filtration (35 mg, 46% yield).

**PCN-223:**[11] $ZrCl_4$ (7 mg, 0.003 mmol), $H_2TCPP$ (10 mg, 0.013 mmol) and acetic acid (0.7mL, 12.24 mmol) in 2 mL of DMF were ultrasonically dissolved in a 4 mL Pyrex vial. The mixture was heated in 120 ºC oven for 12 h. After cooling down to room temperature, needle shaped crystals were harvested by filtration.

### General procedure for PCN-224-M:

In a general procedure is followed the same conditions as for the synthesis of PCN-224 but with the corresponding MTCPP. 0.582 mmol of $ZrOCl_2 \cdot 8H2O$ and 0.047 mmol MTCPP were dissolved in DMF (150 mL) via sonication. Acetic acid (37 mL, 647 mmol) was added, and the mixture was sonicated again. The reaction mixture was heated in an oven (72 h, 65 °C), washed with DMF and resuspended in DMF. The activation procedure is the same as for PCN-224.

### S 2.2.3. STABILITY UNDER ELECTROCHEMICAL CONDITIONS

Electrolyte stability experiments were carried out by immersing 2 mg of MOF-525, PCN-224 and PCN-226 in 2 mL of aqueous solutions of $KHCO_3$ (0.5 M) or $Na_2SO_4$ (0.1 M) at room temperature. The supernatants of MOF-525, PCN-224 and PCN-226 solids soaked in both electrolytes for 0 and 24 hours were analyzed by ICP-MS (**Figures S1 & S2**). All materials soaked in $KHCO_3$ electrolyte show high values of metal leaching which is indicative of a material decomposition. Contrary, MOFs soaked in the $Na_2SO_4$ electrolyte showed lower values of metal leaching being the PCN-224 the most stable.

**Method 1 ($CO_2RR$):**

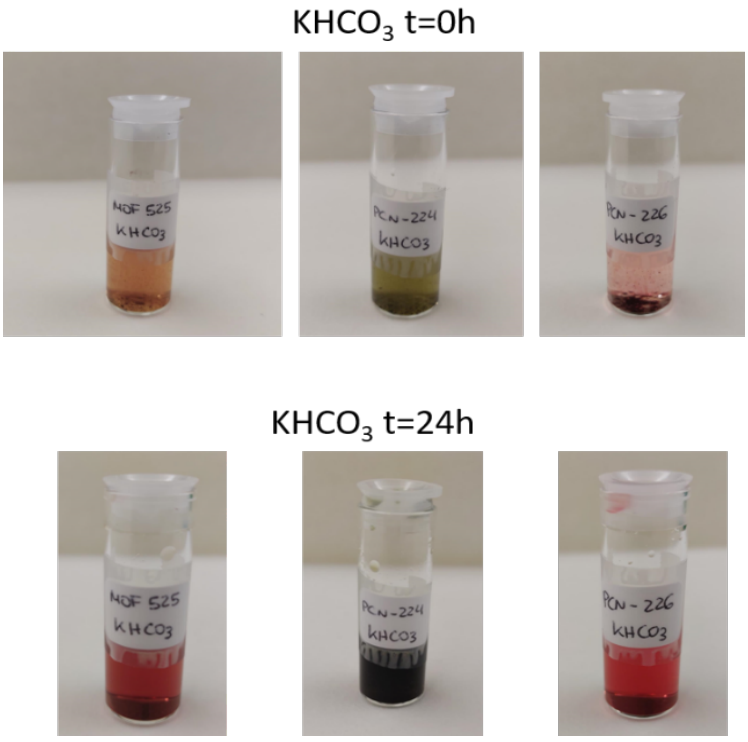


**Figure S7.** Stability of MOF-525, PCN-224 and PCN-226 in $KHCO_3$ electrolyte at time 0 and after 24h to determine the amount of the MOF in solution by ICP.

**Method 2 (NRR):**

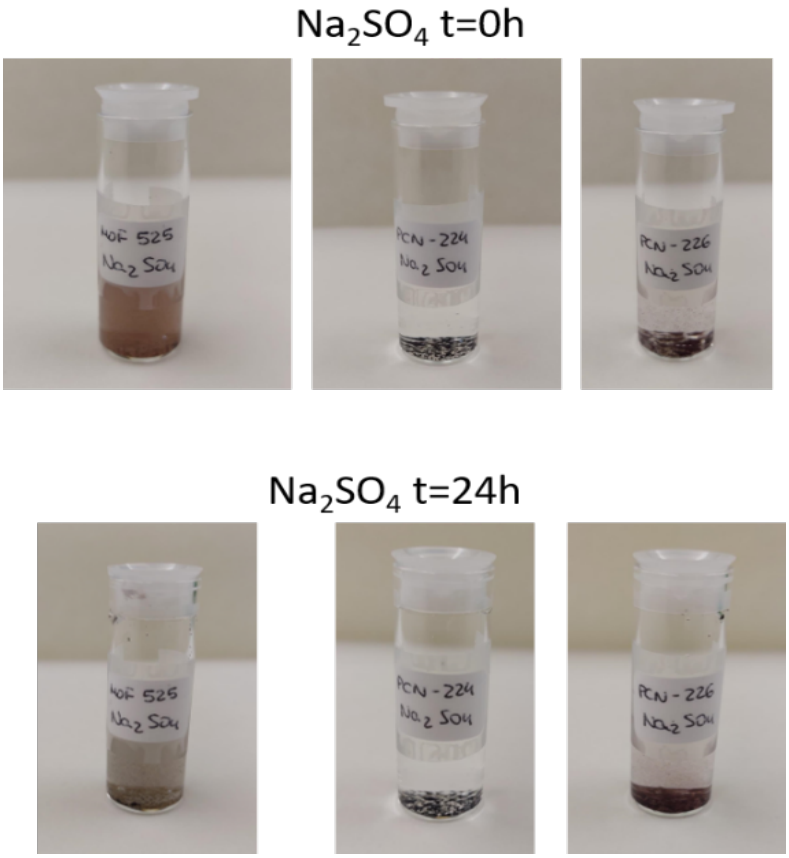


**Figure S8.** Stability of MOF-525, PCN-224 and PCN-226 in $Na_2SO_4$ electrolyte at time 0 and after 24h to determine the amount of the MOF in solution by ICP.

# S3. CHARACTERIZATION OF PCN-224-M

## S3.1. POWDER X-RAY DIFFRACTION

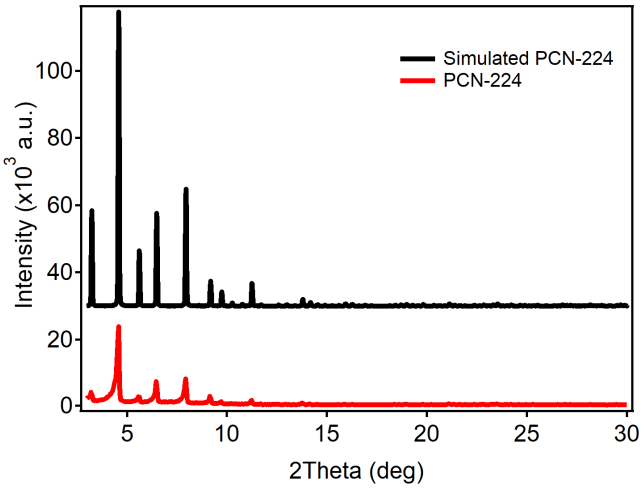


**Figure S9.** PXRD of the simulated PCN-224 and the one synthesized in the lab.

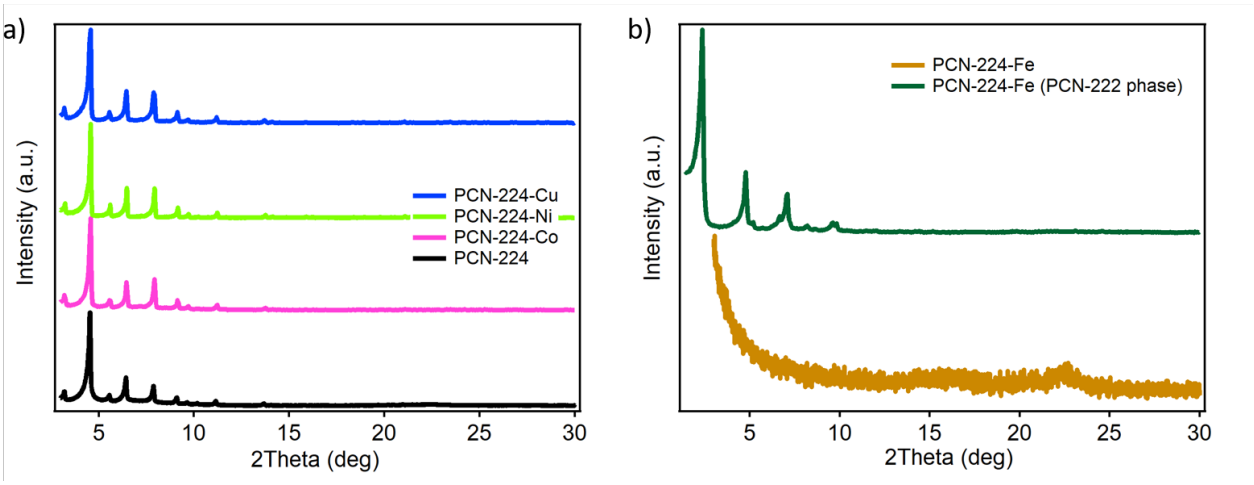


**Figure S10.** PXRD of a) PCN-224 and PCN-224-M pure phases and b) PCN-224-Fe the amorphous and the PCN-222 phases.

## S3.2. SCANNING ELECTRON MICROSCOPY AND ENERGY-DISPERSIVE X-RAY ANALYSIS

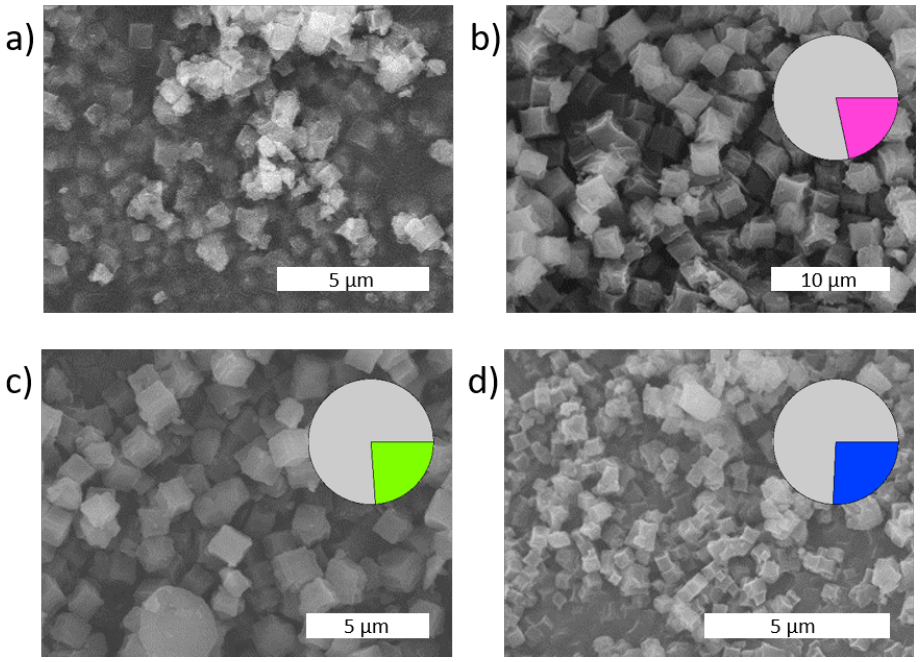


**Figure S11.** SEM images and EDX (pie charts) of a) PCN-224, b) PCN-224-Co, c) PCN-224-Ni, d) PCN-224-Cu. Pie chart color code: Zr, grey; Co, pink; Ni, green; Cu, blue.

## S3.3. NITROGEN ADSORPTION

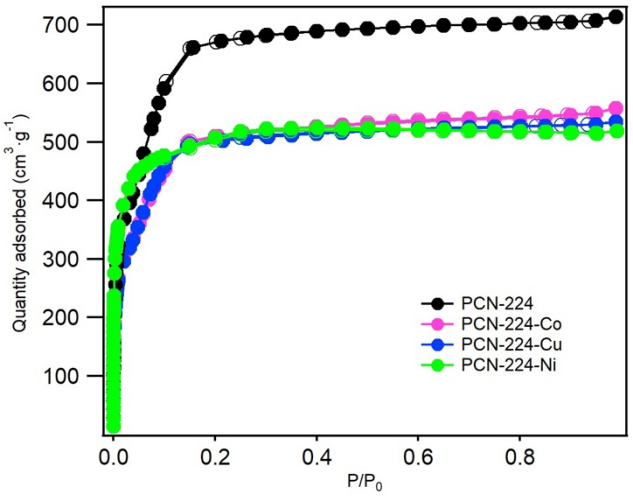


**Figure S12.** $N_2$ isotherms of PCN-224 and PCN-224-M.

**Table S1.** Surface areas and pore volumes comparison.

| MOF | BET ($m^2/g$) | Pore Volume ($cm^3/g$) |
|---|---|---|
| PCN-224 | 2 278.5 | 0.49 |
| PCN-224-Ni | 1 681.6 | 0.28 |
| PCN-224-Cu | 1 660.2 | 0.26 |
| PCN-224-Co | 1 747.9 | 0.25 |

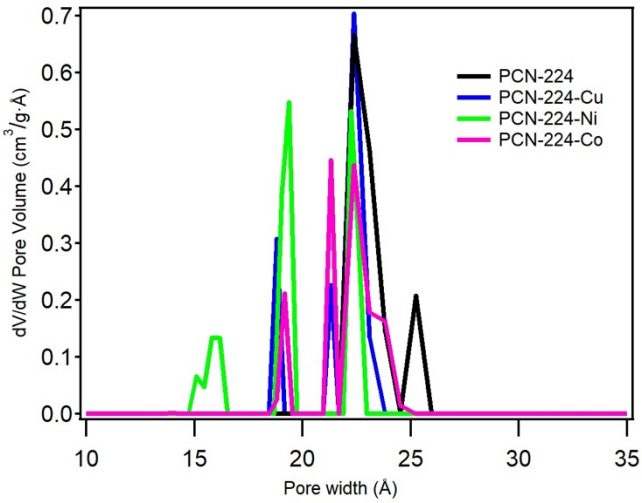


**Figure S*13*.** Pore size distribution plots calculated with a NLDFT kernel from the experimental isotherms of PCN-224 and PCN-224-M.

# S4. CHARACTERIZATION OF PCN-224-Ni(F)

## S4.1. POWDER X-RAY DIFFRACTION

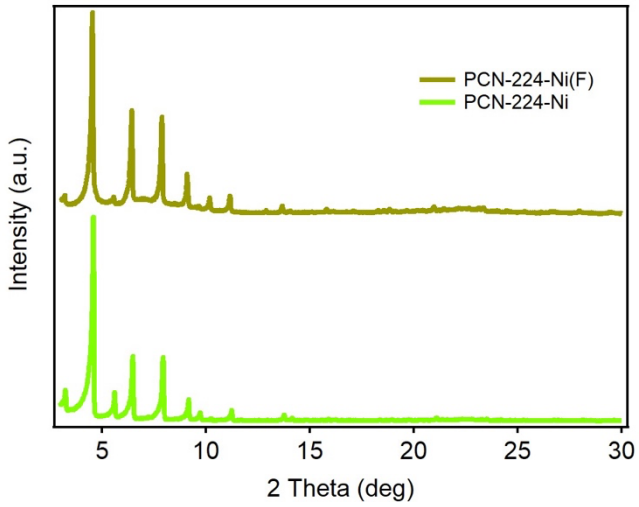


**Figure S14.** PXRD of PCN-224-Ni and PCN-224-Ni(F).

## S4.2. SCANNING ELECTRON MICROSCOPY AND ENERGY-DISPERSIVE X-RAY ANALYSIS

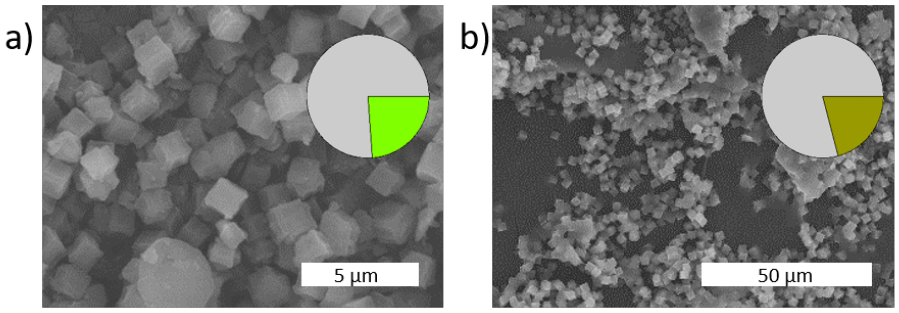


**Figure S15.** SEM images and EDX (pie charts) of a) PCN-224-Ni, b) PCN-224-Ni(F). Pie chart color code: Zr, grey; Ni, green or brown.

## S4.3. NITROGEN ADSORPTION

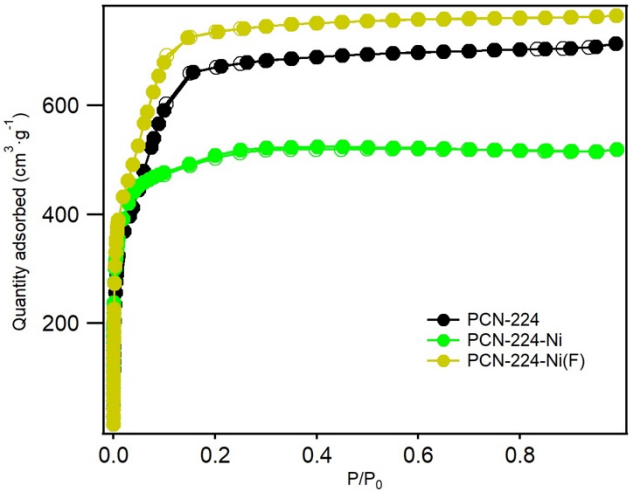


**Figure S16.** $N_2$ isotherms of PCN-224, PCN-224-Ni and PCN-224-Ni(F).

**Table S2.** Surface areas and pore volumes comparison.

| MOF | BET ($m^2/g$) | Pore Volume ($cm^3/g$) |
|---|---|---|
| PCN-224 | 2 278.5 | 0.49 |
| PCN-224-Ni | 1 681.6 | 0.28 |
| PCN-224-Ni(F) | 1 933.6 | 0.52 |

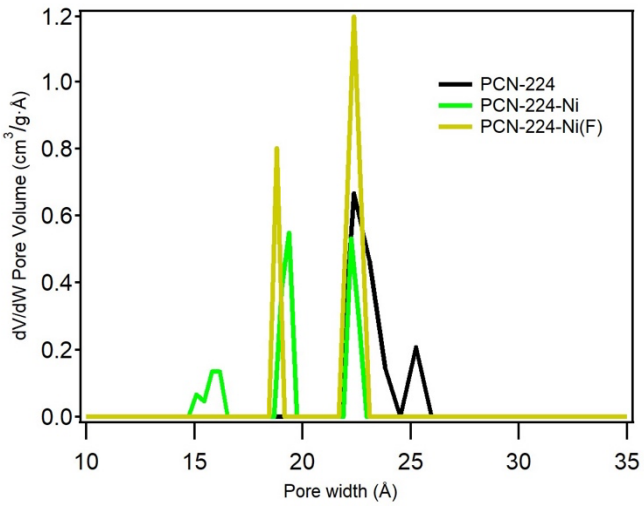


**Figure S17.** Pore size distribution plots calculated with a NLDFT kernel from the experimental isotherms of PCN-224, PCN-224-Ni and PCN-224-Ni(F).

## S4.4. INFRARED SPECTROSCOPY

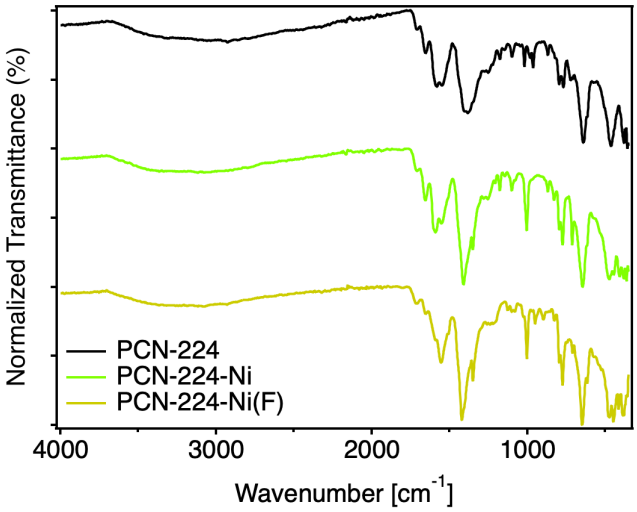


**Figure S18.** FT-IR spectra of PCN-224, PCN-224-Ni and PCN-224-Ni(F).

# S5. CHARACTERIZATION OF PCN-226

## S5.1. POWDER X-RAY DIFFRACTION

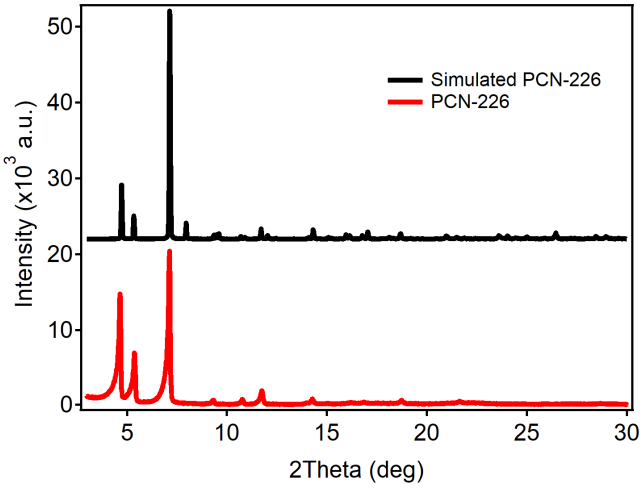


**Figure S19.** PXRD of the simulated PCN-226 and the one synthesized in the lab.

## S5.2. SCANNING ELECTRON MICROSCOPY

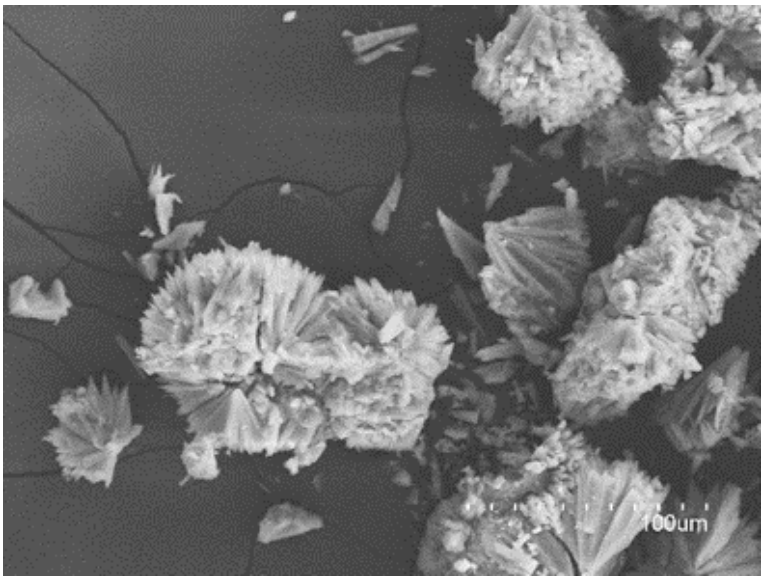


**Figure S20.** SEM image of PCN-226.

## S5.3. NITROGEN ADSORPTION

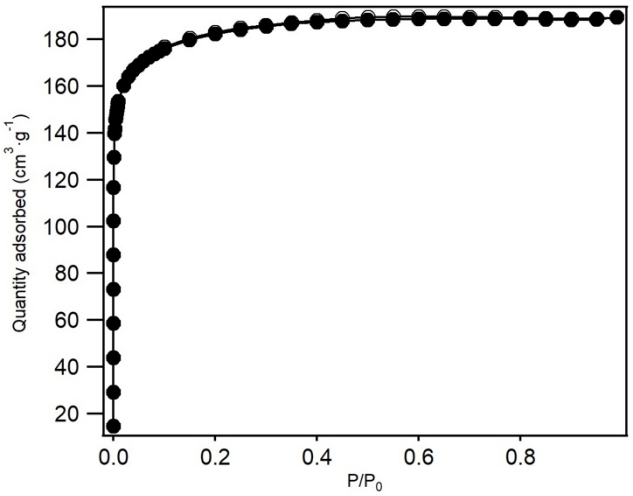


**Figure S21.** $N_2$ isotherm of pcn-226.

# S6. CHARACTERIZATION OF MOF-525

## S6.1. POWDER X-RAY DIFFRACTION

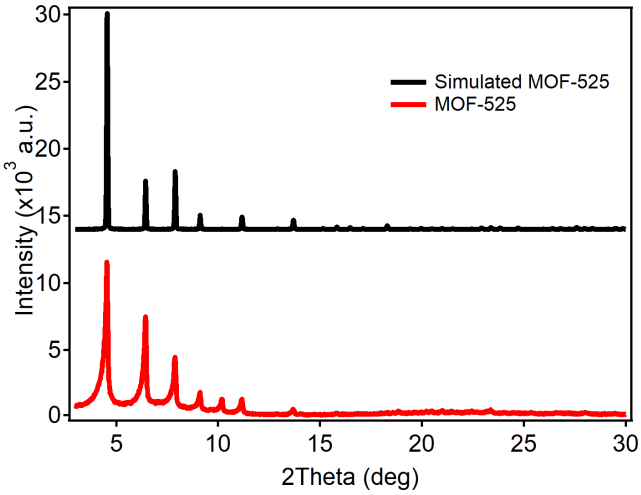


**Figure S22.** PXRD of the simulated MOF-525 and the one synthesized in the lab.

## S6.2. SCANNING ELECTRON MICROSCOPY

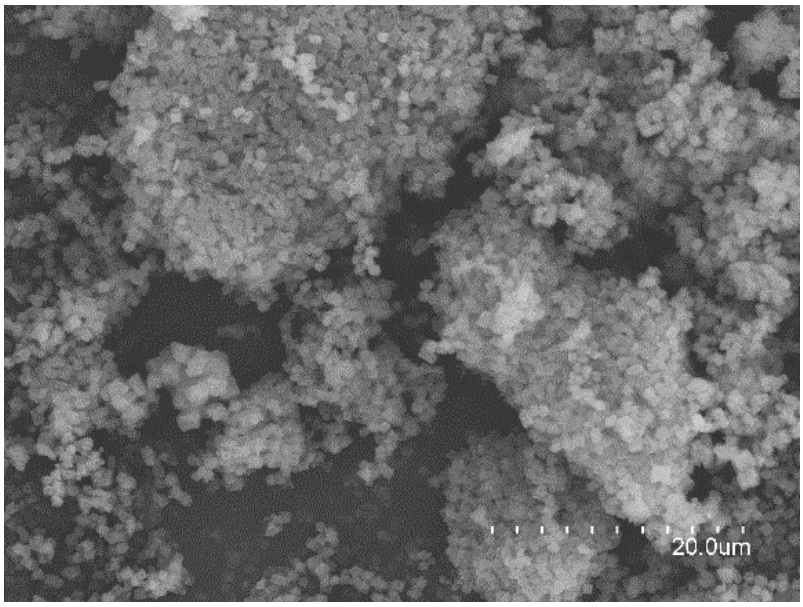


**Figure S23.** SEM image of MOF-525.

## S6.3. NITROGEN ADSORPTION

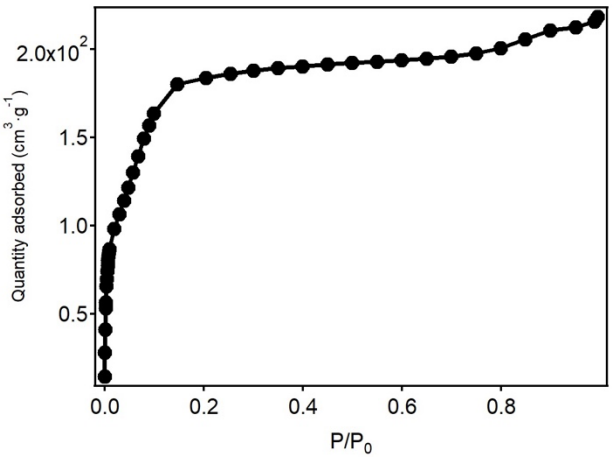


**Figure S24.** $N_2$ isotherm of MOF-525.

# S7. NITROGEN ELECTROREDUCTION

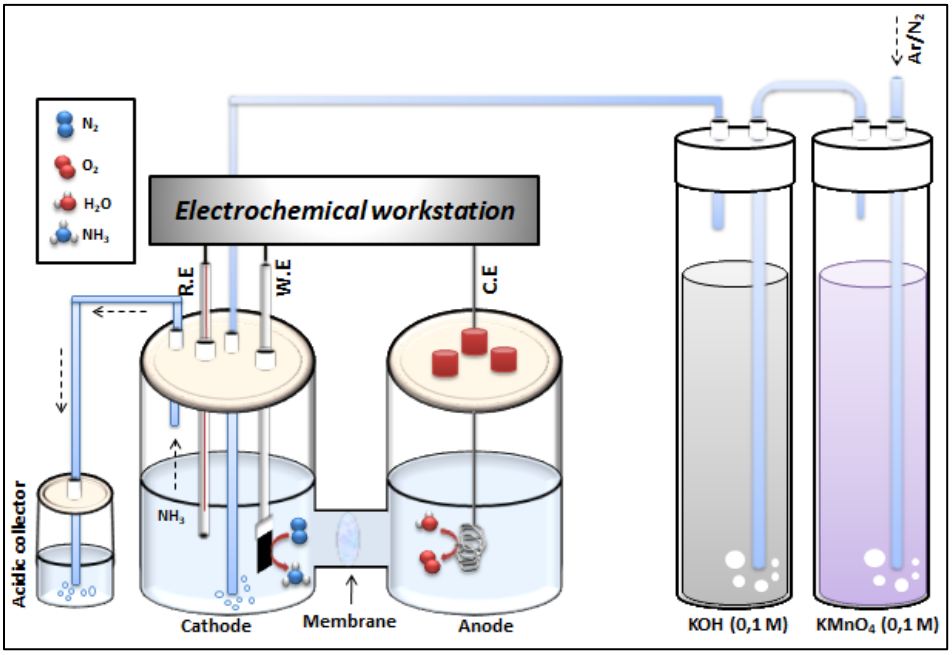


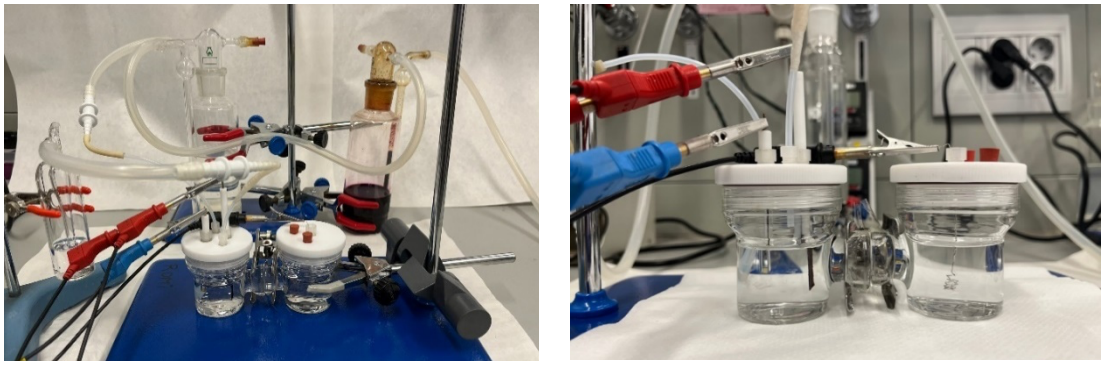

**Figure S25.** Schematic representation and experimental setup used for the electrochemical NRR experiments.

## S7.1. ANALYTICAL DETERMINATION AND ESTIMATION OF FARADAIC EFFICIENCY AND AMMONIA YIELD

The amounts of ammonia produced in both electrochemical cell and acidic trap electrolytes are measured by the "Indophenol blue" method[12] using a HACH Lange DR-3800 system. After 2 h of electrolysis of gaseous $N_2$, 5 mL from the cathodic chamber and the acidic collector were pipetted out and added to the commercial analysis tubes from (LCK 304 Ammonium), where ammonium ions react at pH 12.6 with hypochlorite ions and salicylate ions in the presence of sodium nitroprusside as a catalyst to form indophenol blue, the analysis tubes were kept in the dark for 15 minutes before UV–vis spectrophotometric measurements. The calculation of faradaic efficiency (FE) and ammonia yield rate $r(NH_3)$ was carried out using the next equations:

**Faradaic efficiency** (FE):

$$FE = \frac{3F \times m\,(NH_3)}{17 \times Q} \times 100$$

**Ammonia yield rate** $r(\mathrm{NH_3})$:

$$r(NH_3) = \frac{[\mathrm{NH_4^+}] \times \mathrm{V}}{t \times m(cat)}$$

Where F is the Faraday constant (96485 C/mol); $m(NH_3)$ is the concentration of ammonia in the electrolyte (mol); Q is the amount of electricity consumed in the electrolysis process (C); $[NH_4^+]$ is the concentration of ammonia in the electrolyte (μg $mL^{-1}$); V is the volume of the electrolyte (mL); t is the reduction time (h); $m(\mathrm{cat})$ is the loaded mass of catalyst on carbon paper (mg).

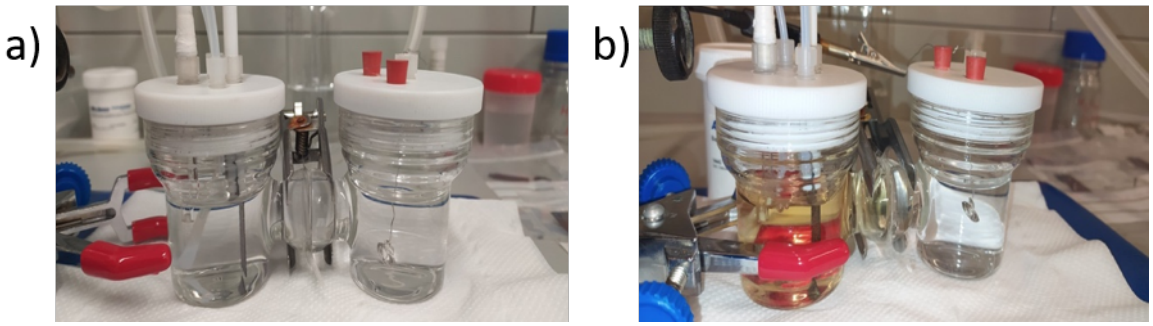


**Figure S26**. a) PCN-224-Ni and b) PCN-224-Co after the electrocatalytic measurements.

**Table S3.** Faradaic Efficiency (FE) and yield (r) measured at negative potentials for all our materials in 0.1 M $Na_2SO_4$ electrolyte for NRR.

| MOF-based catalyst | Potential vs RHE | FE % | $r_{NH3}$ μg $h^{-1}$ $mg^{-1}$ |
|---|---|---|---|
| PCN-224-Co | -0.04 V | 11.37 | 0.60 |
| | -0.14 V | 5.75 | 0.24 |
| | -0.34 V | 4.46 | 0.20 |
| PCN-224-Ni | -0.04 V | 32.29 | 0.77 |
| | -0.14 V | 6.00 | 0.34 |
| | -0.34 V | 3.93 | 0.25 |
| PCN-224-Cu | -0.04 V | 21.73 | 0.50 |
| | -0.14 V | 10.23 | 0.31 |
| | -0.34 V | 4.36 | 0.23 |
| PCN-224-Ni(F) | -0.04 V | 34.50 | 0.90 |
| | -0.14 V | 19.71 | 0.70 |
| | -0.34 V | 5.91 | 0.31 |

**Table S4.** Faradaic Efficiency of different MOFs used in NRR.

| **MOF-based catalyst** | **Electrolyte** | **Potential vs RHE** | **FE%** | **Ref.** |
|---|---|---|---|---|
| FeNi2S4/NiS | 0.1M KOH | -0.3V | (28.64 ± 0.18%) | 13 |
| ZIF-67@Ti3C2 | 0.1M KOH | -0.4V | 20.2% | 14 |
| UiO-66 | 0.1 M $Na_2$ $SO_4$ | -0.3V | 48.06% | 15 |
| Au@MOF | 0.1 M $Na_2$ $SO_4$ | -0.3V | 60.9% | 16 |
| S/N-MPC | 0.05 M $H_2SO_4$ | -0.2V | 25.16% | 17 |
| CNT@MIL-101(Fe) | 0.05 M $H_2SO_4$ | -0.4V | 37.28% | 18 |
| Zn−Co3O4 | 0.1 M HCl | -0.3V | 11.9% | 19 |
| MoP@PPC | 0.1 M HCl | -0.3V | 2.48% | 20 |
| C@NiO@Ni | 0.1M KOH | -0.7V | 10.9% | 21 |
| CoxFe–MOF | 0.1 M HCl | -0.2 V | 25.64% | 22 |
| C@YSZ | 0.1 M $Na_2$ $SO_4$ | -0.5 V | 8.2% | 23 |
| ZIF-derived carbon | 0.1M KOH | -0.3V | 10.2% | 24 |
| Bi-CeO2 | 0.5M K2SO4 | -0.5V | 8.56% | 25 |
| $Fe_1$-N-C | 0.1 M HCl | -0.05V | 4.51% | 26 |
| hC-VC | / | -0.1V | 18.3% | 27 |
| Fe–TCPP MOFs | 0.1 M HCl | -0.5 V | 16.23% | 28 |
| Bi-MOF | 0.10 M $Na_2SO_4$ | −0.6 V | 12.11 ± 0.84% | 29 |
| PCN-222(Fe) | 0.1 M HCl | 1.6 V | 70.7% | 30 |

## S7.2. ASSESSMENT OF OBTAINED RESULTS AND STABILITY OF THE ELECTRODES

Several blank and control experiments were systematically and routinely performed to demonstrate that the $NH_3$ obtained comes from the electrocatalytic reduction of $N_2$ rather than from impurities. Electrolysis experiments were performed replacing $N_2$ by Ar. The absence of ammonia in the analyses guarantees the

absence of reactive impurities for the electrochemical formation of ammonia as well as the absence of ammonia from the materials and chemicals used in the experiments. This control experiment enables the identification of potential sources of contamination such as the glassery, the membrane and the electrodes, facilitating cleaning them prior to further usage. It is worth mentioning that these blank/control experiments are systematically run both before the beginning of a new series of experiments and during the intervals between successive experiments with positive results. In this way, a positive result is always placed between two blank experiments with negative results (in term of ammonia detection). Additionally, other control experiments were performed by bubbling only $N_2$ gas through the electrochemical cell in the absence of electrodes and, obviously, potential control. This control experiment is of outstanding importance to guarantee the absence of NOx contaminations in the flow of $N_2$ that enters the electrochemical system from the $N_2$ gas cylinder. These results ensured that the $NH_3$ produced is derived from the electrochemical NRR.

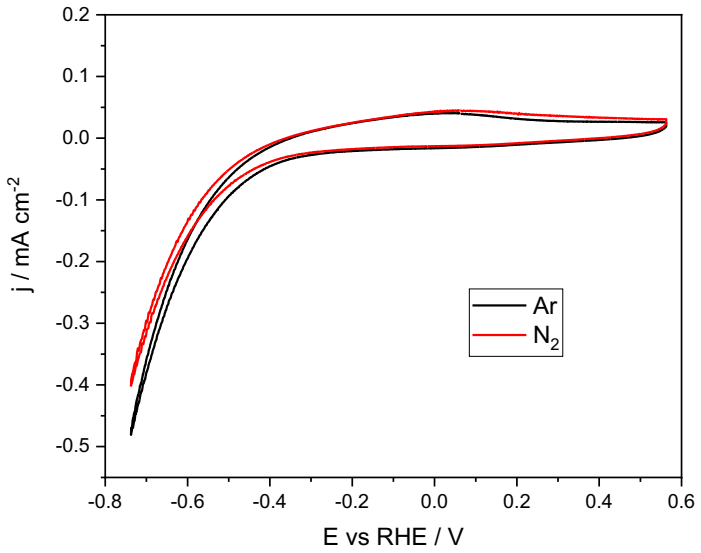


**Figure S27.** Voltammetric profile of a Toray paper (TGPH-90) electrode in Ar (black line) and $N_2$ (red line) saturated 0.1 M $Na_2SO_4$ solution. Scan rate 50 mV $s^{-1}$.

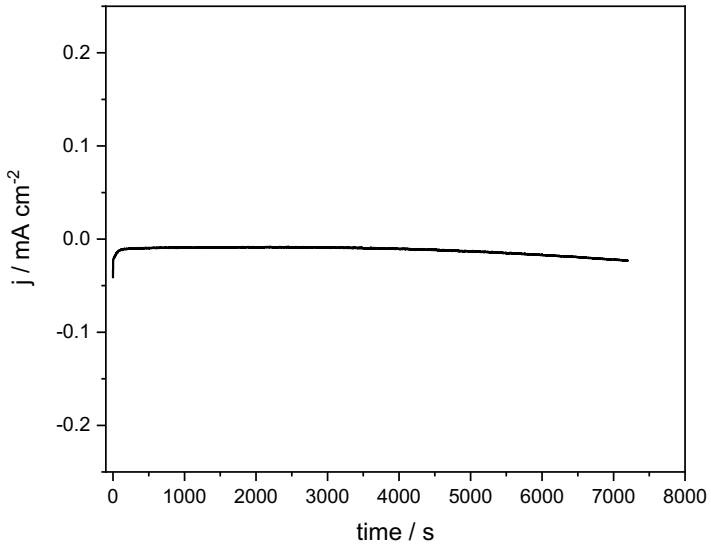


**Figure S28.** Chronoamperometric measurements at -0.04 V vs RHE with a Toray paper (TGPH-90) electrode in a $N_2$-saturated 0.1 M $Na_2SO_4$ solution.

# S8. WATER ADSORPTION

For additional effects on the improvement of recyclability recorded we also analysed the water uptake of PCN-224-Ni and PCN-224-Ni(F). The data below show the significant differences in water uptake for both solids at 298 K.

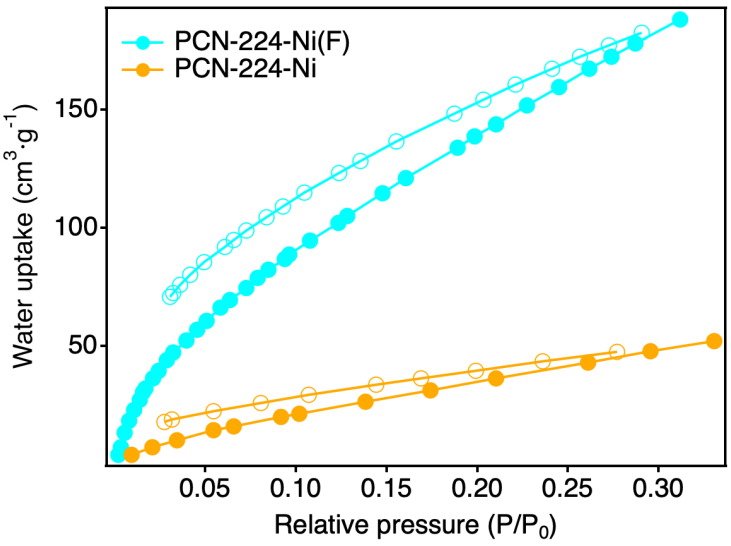


**Figure S29.** Water isotherms of PCN-224-Ni and Ni(F) measured at 298 K. We associate this different behaviour to the enhanced stability of the fluorinated framework that is less prone to collapse due to fluorine functionalization.

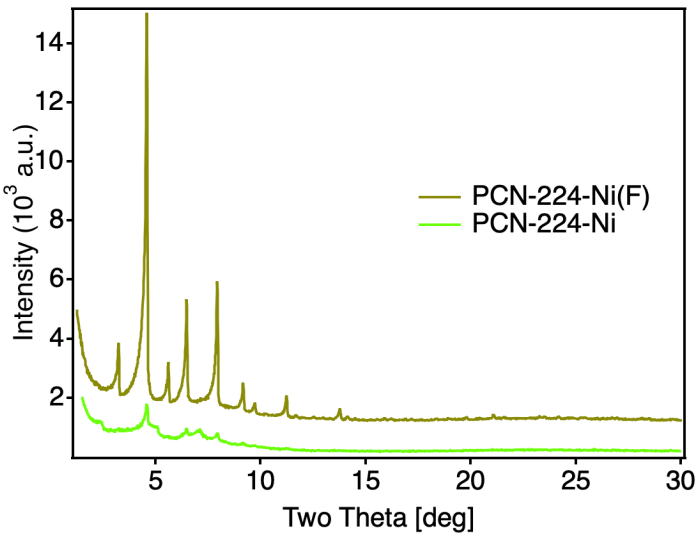


**Figure S30.** PXRD of PCN-224-Ni and PCN-224-Ni(F) after incubation in $Na_2SO4$ for 24 h.

# S9. COMPUTATIONAL SECTION

To understand the activity of PCN-224-M in the electroreduction of $N_2$, we performed the DFT calculations for density of states of MTCPP-X (M = Ni, Co, Cu and X = H, F) and adsorption energy of the reactant, using VASP code[31,32] and the MOF systems were represented by cluster models. The electron–ion interactions were described using the projector-augmented-wave (PAW) formalism.[33] For the geometry optimizations, we used the generalized gradient approximation (GGA) with the Perdew–Burke–Ernzerhof (PBE) functional,[34] and including van der Waals (vdW) corrections via the DFT-D3 method of Grimme.[35] The kinetic energy cut-off for the plane-wave basis set expansion was chosen as 500 eV, and a Γ-points was used. he screened hybrid functional (HSE06)[36] was then used for single-point calculations at the PBE equilibrium geometries, in order to obtain more accurate electronic structures.

**Table S5.** Summary of calculated HOMO-LUMO values of family of cluster of M-TCPP-X.

| M-TCPP-X | HOMO | LUMO |
|---|---|---|
| Co-TCPP-H | -4.9 | -2.3 |
| Cu-TCPP-H | -4.9 | -2.5 |
| Ni-TCPP-H | -5.1 | -2.5 |
| Ni-TCPP-F | -4.9 | -2.4 |

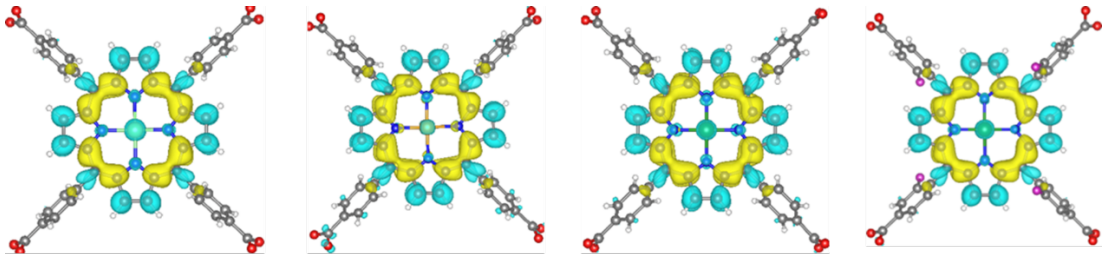


**Figure S31.** Their corresponding density of state are plotted.

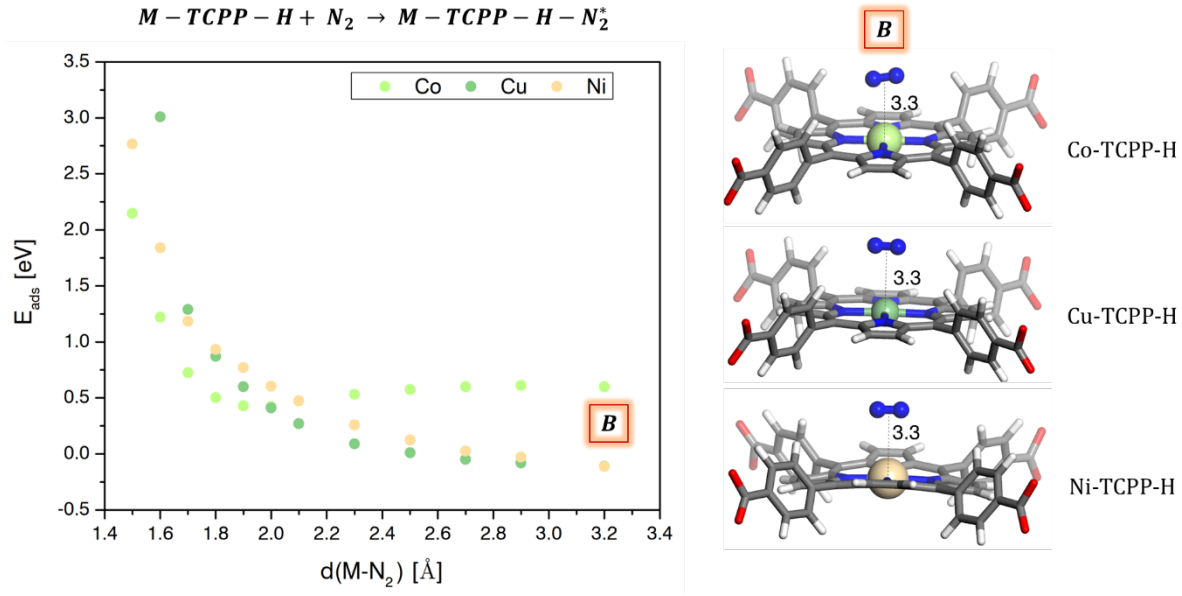


**Figure S32.** Adsorption energy ($E_{ads}$, in eV) for $N_2$ adsorption at different distances from the metal centre of the porphyrins (left) and the optimised more stable structure (right).

Tafel-Volmer mechanism is described by the following equations:

Hydrogen dissociation:

$$^1/_2\, H_2 \rightarrow H^+ + e^- \quad (1)$$

Electron transfer to the systems:

$$M - TCPP - X + e^- \rightarrow [M - TCPP - X]^- \quad (2)$$

Adsorption energy of $H^+$:

$$[M - TCPP - X]^- + H^+ \rightarrow M - HTCPP - X \quad (3)$$

Adsorption energy of $N_2$:

$$M - HTCPP - X + N_2 \rightarrow M - HTCPP - X{-}N_2{}^* \quad (4)$$

**Table S6.** Summary of energy of reaction calculated of steps (2) – (4). All energies in eV.

| MTCPP(X) | (2) | (3) | (4) |
|---|---|---|---|
| CoTCPP(H) | -2.65 | +0.47 | +0.22 |
| CuTCPP(H) | -2.33 | -0.01 | +0.03 |
| NiTCPP(H) | -2.31 | +0.81 | -0.17 |
| NiTCPP(F) | -2.20 | +0.86 | -0.21 |

# S10. REFERENCES


(1) S. Z. Andersen, V. Čolić, S. Yang, J. A. Schwalbe, A. C. Nielander, J. M. McEnaney, K. Enemark Rasmussen, J. G. Baker, A. R. Singh, B. A. Rohr, M. J. Statt, S. J. Blair, S. Mezzavilla, J. Kibsgaard, P. C. K. Vesborg, M. Cargnello, S. F. Bent, T. F. Jaramillo, I. E. L. Stephens, J. K. Nørskov, I. Chorkendorff, *Nature*, 2019, **570**, 504.

(2) J. Choi, B. H. R. Suryanto, D. Wang, H. L. Du, R. Y. Hodgetts, F. M. Ferrero Vallana, D. R. MacFarlane, A. N. Simonov, *Nat. Commun*., 2020, **11**, 5546.

(3) H. Liu, N. Guijarro, J. Luo, *J. Energy Chem*., 2021, **61**, 149.

(4) A. J. Martín, F. L. P. Veenstra, J. Lüthi, R. Verel, J. Pérez-Ramírez, *Chem Catal.*, 2021, **1**, 1505.

(5) Y. Li, Z. Wang, H. Ji, L. Zhang, T. Qian, C. Yan, J. Lu, *Chinese J. Catal*., 2023, **44**, 50.

(6) M. O. Senge, N. N. Sergeeva, K. J. Hale, *Chem. Soc. Rev.,* 2021, **50**, 4730–4789.

(7) C. Koschnick, R. Stäglich, T. Scholz, M. W. Terban, A. von Mankowski, G. Savasci, F. Binder, A. Schökel, M. Etter, J. Nuss, R. Siegel, L. S. Germann, C. Ochsenfeld, R. E. Dinnebier, J. Senker, B. V. Lotsch, *Nat Commun.,* 2021, **12**, 3099.

(8) M. O. Cichocka, Z. Liang, D. Feng, S. Back, S. Siahrostami, X. Wang, L. Samperisi, Y. Sun, H. Xu, N. Hedin, H. Zheng, X. Zou, H. C. Zhou, Z. Huang, *J. Am. Chem. Soc.,* 2020, **142**, 15386-15395.

(9) W. Morris, B. Volosskiy, S. Demir, F. Gándara, P. L. McGrier, H. Furukawa, D. Cascio, J. F. Stoddart, O. M. Yaghi, *Inorg. Chem.,* 2012, **51**, 6443–6445.

(10) D. Feng, Z. Y. Gu, J. R. Li, H. L. Jiang, Z. Wei, H. C. Zhou, *Angew. Chem. Int. Ed.,* 2012, **51**, 10307–10310.

(11) D. Feng, Z. Y. Gu, Y. P. Chen, J. Park, Z. Wei, Y. Sun, M. Bosch, S. Yuan, H. C. Zhou, *J. Am. Chem. Soc.,* 2014, **136**, 17714–17717.

(12) D. Li, X. Xu, Z. Li, T. Wang, C. Wang, *Trends Anal. Chem*., 2020,**127**, 115890.

(13) P. Y. Liu, K. Shi, W. Z. Chen, R. Gao, Z. L. Liu, H. Hao, Y. Q. Wang, *Appl. Catal. B Environ.,* 2021, **287**, 119956.

(14) X. Liang, X. Ren, Q. Yang, L. Gao, M. Gao, Y. Yang, H. Zhu, G. Li, T. Ma, A. Liu, *Nanoscale,* 2021, **13**, 2843–2848.

(15) X. He, Y. Liao, J. Tan, G. Li, F. Yin, *Electrochim. Acta,* 2022, **409**, 139988.

(16) H. He, Q. Q. Zhu, Y. Yan, H. W. Zhang, Z. Y. Han, H. Sun, J. Chen, C. P. Li, Z. Zhang, M. Du, *Appl. Catal. B Environ.,* 2022, **302**, 120840.

(17) J. Wang, H. Huang, P. Wang, S. Wang, J. Li, *Carbon,* 2021, **179**, 358–364.

(18) Y. Lv, Y. Wang, M. Yang, Z. Mu, S. Liu, W. Ding, M. Ding, *J. Mater. Chem. A,* 2021, **9**, 1480–1486.

(19) L. Wen, X. Li, R. Zhang, H. Liang, Q. Zhang, C. Su, Y. J. Zeng, *ACS Appl. Mater. Interfaces,* 2021, **13**, 14181–14188.

(20) J. Duan, D. Shao, W. Wang, D. Zhang, C. Li, *Microporous Mesoporous Mater.,* 2021, **313**, 110852.

(21) S. Luo, X. Li, W. Gao, H. Zhang, M. Luo, *Sustain. Energy Fuels,* 2019, **4**, 164–170.

(22) W. Li, W. Fang, C. Wu, K. N. Dinh, H. Ren, L. Zhao, C. Liu, Q. Yan, *J. Mater. Chem. A,* 2020, **8**, 3658–3666.

(23) S. Luo, X. Li, M. Wang, X. Zhang, W. Gao, S. Su, G. Liu, M. Luo, *J. Mater. Chem. A,* 2020, **8**, 5647–5654.

(24) S. Mukherjee, D. A. Cullen, S. Karakalos, K. Liu, H. Zhang, S. Zhao, H. Xu, K. L. More, G. Wang, G. Wu, *Nano Energy,* 2018, **48**, 217–226.

(25) Y. Liu, C. Li, L. Guan, K. Li, Y. Lin, *J. Phys. Chem. C,* 2020, **124**, 18003–18009.

(26) R. Zhang, L. Jiao, W. Yang, G. Wan, H. L. Jiang, *J. Mater. Chem. A,* 2019, **7**, 26371–26377.

(27) C. Zhang, D. Wang, Y. Wan, R. Lv, S. Li, B. Li, X. Zou, S. Yang, *Mater. Today,* 2020, **40**, 18–25.

(28) M. Cong, X. Chen, K. Xia, X. Ding, L. Zhang, Y. Jin, Y. Gao, L. Zhang, *J. Mater. Chem. A,* 2021, **9**, 4673–4678.

(29) D. Yao, C. Tang, L. Li, B. Xia, A. Vasileff, H. Jin, Y. Zhang, S. Z. Qiao, *Adv. Energy Mater.,* 2020, **10**, 2001289.

(30) H. He, H. K. Li, Q. Q. Zhu, C. P. Li, Z. Zhang, M. Du, *Appl. Catal. B Environ.,* 2022, **316**, 121673.

(31) G. Kresse, J. Furthmüller, *Comput. Mater. Sci.,* 1996, **6**, 15– 50.

(32) G. Kresse, J. Furthmüller, *Phys. Rev. B Condens. Matter Mater. Phys.,* 1996, **54**, 11169– 11186.

(33) G. Kresse, D. Joubert, *Phys. Rev. B Condens. Matter Mater. Phys.,* 1998, **59**, 1758–1775.

(34) J. P. Perdew, K. Burke, M. Ernzerhof, *Phys. Rev. Lett.,* 1996, **77**, 3865– 3868.

(35) S. Grimme, J. Antony, S. Ehrlich, H. Krieg, *J. Chem. Phys.,* 2010, **132**, 154104.

(36) J. Heyd, G. E. Scuseria, M. Ernzerhof, *J. Chem. Phys.,* 2003, **118**, 8207– 8215.